Journal of Alloys and Compounds 509 (2011) 8401–8406

Contents lists available at ScienceDirect

Journal of Alloys and Compounds

journal homepage: www.elsevier.com/locate/jallcom

Solvothermally synthesized tungsten oxide nanowires/nanorods for NO_2 gas sensor applications

Yuxiang Qin*, Xiao Li, Fei Wang, Ming Hu

School of Electronics and Information Engineering, Tianjin University, No. 92, Weijin Road, Nankai District, Tianjin 300072, PR China

ARTICLE INFO

Article history:
Received 15 February 2011
Received in revised form 5 May 2011
Accepted 26 May 2011
Available online 6 June 2011

Keywords:
Tungsten oxide
Nanostructure
NO_2
Gas sensor

ABSTRACT

One-dimensional nanorods or nanowires of $W_{18}O_{49}$ were synthesized by solvothermal method at 200 °C with tungsten hexachloride (WCl_6) as precursor and cyclohexanol or 1-propanol as reaction solvent. Their morphology and structure properties were systematically characterized. The NO_2-sensing properties of the sensors based on nanowires and nanorods were investigated at 100 °C up to 250 °C over NO_2 concentration ranging from 1 ppm to 20 ppm. The results indicate that both nanowires and nanorods exhibit reversible response to different concentrations of NO_2, and the highest gas response is achieved at 150 °C. In comparison with nanorods, nanowires showed a much quicker response characteristic and a relative higher response value to the same concentration of NO_2 gas due to the smaller diameter and larger specific surface area.

1. Introduction

Detection of toxic gases such as NO_x, O_3, NH_3, CO, H_2S, and SO_x is important for both environmental protection and human health, and has attached significant research interests. At present, various metal oxide semiconductors including SnO_2, WO_{3-x}, ZnO, MoO_3, and TiO_2, have been widely used for sensing these toxic gases [1–4]. The sensing mechanism lies in the changes in electrical conductivity of metal oxides in the presence of toxic gases and oxygen due to catalytic reduction/oxidation reactions occurring at the metal oxide surface. Therefore, increasing in the active surface area of the semiconductor oxide leads to enhancement of sensing-properties for supplying a large amount of surface active sites for gas adsorption and reaction [5,6]. In recent years, various nanostructured materials such as nanowires, nanotubes, nanorods and nanobelts, have been evaluated as ideal candidates for gas sensor applications due to their large specific surface areas and dimensions comparable to Debye length [7,8]. In fact, gas sensing materials such as tin oxide [9], titanium oxide [10], zinc oxide [11] and indium oxide [12] with well-established nanostructure have shown higher sensitivity and quicker response in gas detection at low concentrations than their corresponding thin film materials [13,14].

Through an extensive research for various metal oxide semiconductors, tungsten oxide (WO_{3-x}), which is a wide band-gap n-type semiconductor, has been found to be a promising material for toxic gases detection [15,16]. So far, extensive studies have been conducted on tungsten oxide sensing materials based on nanocrystalline powders or films. Since metal oxide-based gas sensors usually work at temperatures ranging from 200 °C to 400 °C, annealing step is necessary to stabilize the sensing films microstructure. However, the decrease of the active surface area, resulted from nanocrystalline growth and structural pores shrinkage during annealing treatment, should not be ignored for sensing materials with nanocrystalline structure [17,18]. In recent studies, one- and two-dimensional tungsten oxide nanostructures such as nanowires, nanosheets and nanotubes were investigated and good sensing-properties for detecting toxic and hazardous gases were observed. Chen et al. [19] reported that single-crystalline potassium-doped tungsten oxide nanosheets showed high sensitivity, fast response time and good stability to H_2S, acetone and Cl_2. The investigation of Rao et al. [20] indicated that $WO_{2.72}$ nanowires had much higher response value to H_2S than nanoparticles or nanoplatelets of WO_3. Very recently, Benkstein et al. [21] reported that sensor based on tungsten oxide nanotubes could detect dilute NO_2 as low as 200 ppb at 200 °C and exhibited response two to three orders-of-magnitude higher than the one based on WO_3 thin film. These results clearly demonstrate the potential of tungsten oxide nanostructures in toxic gas detection. In this work, nanorods and nanowires of tungsten oxide were synthesized by solvothermal method in different solvents, and their microstructures were systematically characterized. Also, the sensing characteristics of the nanorods and nanowires towards NO_2 gas ranging from 1 to 20 ppm at operating temperature of 100–250 °C were investigated. Our study shows that the one-dimensional tungsten oxide can exhibit good response characteristics to NO_2 gas, as described below.

* Corresponding author. Tel.: +86 22 27402372; fax: +86 22 27401233.
E-mail address: qinyuxiang@tju.edu.cn (Y. Qin).

0925-8388/$ – see front matter © 2011 Elsevier B.V. All rights reserved.
doi:10.1016/j.jallcom.2011.05.100

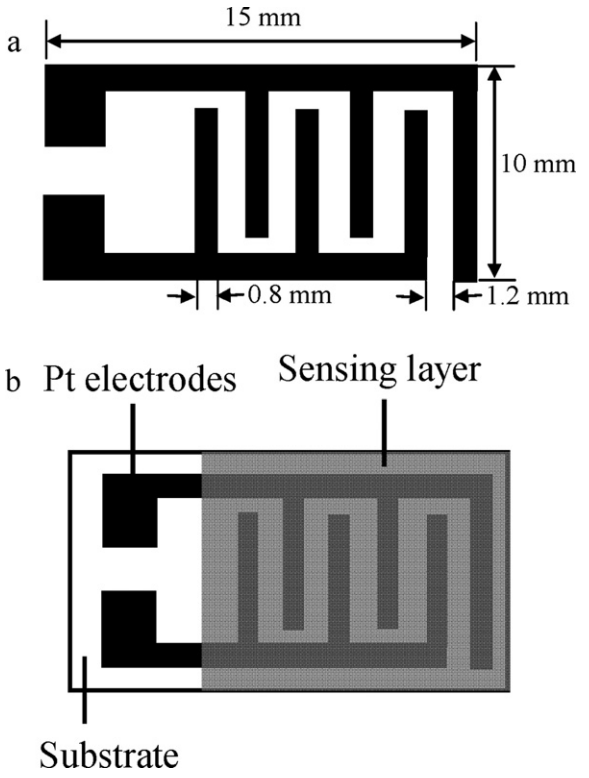

Fig. 1. Schematic diagrams of the interdigitated Pt electrodes (a) and the sensor (b).

2. Experimental

2.1. Synthesis of tungsten oxide nanowires/nanorods

Nanorods and nanowires of tungsten oxide were synthesized by solvothermal method with tungsten hexachloride (WCl_6) as precursor. In a typical procedure to prepare tungsten oxide nanorods, a certain amount of WCl_6 was dissolved in a little ethanol in a beaker to obtain a solution. The ratio of WCl_6 mass to ethanol volume is 0.1 g/ml. Cyclohexanol was then added to this solution, which was subsequently transferred to and sealed in a 100 ml Teflon-lined stainless steel autoclave. The concentration of WCl_6 in cyclohexanol was maintained constant at 0.005 M in our experiments. The solvothermal reaction was conducted at 200 °C for 6 h in an electric oven. After that, the autoclave was cooled naturally to room temperature. The final products were centrifuged and washed sequentially with deionized water and ethanol for several times, and the obtained powder was dried at 70 °C for 6 h in air. Very similar to the above procedure, to prepare tungsten oxide nanowires, 1-propanol was added as solvent instead of cyclohexanol and the reaction time was prolonged to 9 h. Note that there was no any precipitate obtained in 1-propanol when reacting for 6 h. All other conditions were held unchanged to prepare tungsten oxide nanorods.

2.2. Characterization

The morphology, crystal structure, and phase composition of the tungsten oxides were characterized by using a field emission scanning electron microscope (FESEM, FEI Nanosem 430), an X-ray diffractometer (XRD, RIGAKU D/MAX 2500V/PC, Cu Kα radiation) and a field emission transmission electron microscope (FETEM, TECNAI G^2F-20). X-ray photoelectron spectroscopy (XPS) (PERKIN ELEMER PHI-1600 ESCA) was used to investigate the chemical state of the tungsten oxide nanostructures. XPS W4f core level spectra were measured for the tungsten oxide nanowire and nanorod films spin-coated on the silicon substrates after annealing at 300 °C for 1 h at ambient atmosphere. The thickness of the film was less than 1 μm. In order to evaluate the specific surface area of the products, Brunauer–Emmett–Teller (BET) gas-sorption measurements were carried out by using Quantachrome NOVA automated gas sorption system after the samples were vacuum-dried at 200 °C for 10 h.

2.3. Sensor preparation and measurement

The gas sensors were fabricated by spin coating the slurry of synthesized tungsten oxide nanostructures on the cleaned alumina substrates which were attached with a pair of interdigitated Pt electrodes in 100 nm thickness. The electrodes were deposited by using RF magnetron sputtering method. Fig. 1(a) and (b) shows the schematic diagrams of the interdigitated electrodes and the sensor respectively. The coating slurry was prepared by ultrasonically dispersing tungsten oxide powders in mixed organic solvents of terpineol and ethanol with 2:1 volume ratio for 2 h. During the spin coating, the rotating speed was gradually increased to 1500 rpm for 30 s. A physical mask was used to avoid the presence of slurry at the end of the substrate. The coated sensing films were subsequently annealed at 300 °C for 1 h at ambient atmosphere in a program-controlled furnace in order to burn out the organic vehicle (i.e. terpineol) used in the preparation of the coating slurry as well as to enhance the adherence of the sensing film to the sensor substrates. Temperature was raised from ambient to 300 °C using a slow ramp of 2.5 °C/min in order to avoid the occurrence of cracks in the films. After annealing, a sensing film of 10 mm × 10 mm in size and ~1 μm in thickness was formed. During preparation of nanowires and nanorods sensor samples, similar thickness of sensing layers was ensured by stable control of the spin-coating conditions.

The NO_2 gas sensing measurements were carried out in a home-built static gas sensing characterization system consisting of a 30 L glass test chamber with a movable top cover, a flat heating plate with a temperature controller, a programmable digital multimeter and a data acquisition system. The sensors were placed on the heating plate fixed in the test chamber. Pure NO_2 gas was introduced into the test chamber by static volumetric method. That is, a predetermined amount of gas was injected into the chamber directly by a micro-injector to get the desired concentration. The sensors were recovered by opening the top cover of the test chamber and setting up the electric blower fixed at the bottom of the chamber. During the whole measurement process, the programmable professional digital multimeter (UNI-T UT70D) controlled by a personal computer was used for continuously monitoring the resistance changes of the sensors during the whole measurement process. The sampling interval was set to 1 s, and the acquired resistance data was stored in a computer for further analysis. The operating temperature of the sensing films was changed from 150 to 250 °C by adjusting the temperature controller of the heating plate. The gas response was defined to be R_g/R_0, where R_g and R_0 are the resistances of a sensitive film in a measuring gas and that in clean air, respectively.

3. Results and discussion

3.1. Structure characterization

Fig. 2(a)–(d) respectively shows the morphologies of tungsten oxide nanostructures synthesized in the solvents of cyclohexanol and 1-propanol via solvothermal method at 200 °C. The SEM image shown in Fig. 2(a) exhibits that the product obtained in cyclohexanol is mainly composed of short nanorods with diameter of 30–40 nm and length of 300–400 nm. Several thinner nanorods assembled together along the axis direction form nanorod bundles. Fig. 2(b) shows the TEM image of one such nanorod bundle. When substituting cyclohexanol with 1-propanol and prolonging reaction time to 9 h, nanowires exhibiting thin and long features were obtained, as shown in Fig. 2(c). Further TEM investigation to these nanowires shown in Fig. 2(d) identified their bundle feature. Shown in the figure, each nanowire in the bundles has diameter of about 10 nm. The formation of nanorod or nanowire bundles might result from the hydrogen bonding interaction between the thinner nanorods or nanowires [22].

XRD analysis was carried out to identify the crystalline structure of the tungsten oxide nanorods/nanowires after annealing at 300 °C for 1 h (see Fig. 3). As shown in this figure, the XRD patterns of the bundled tungsten oxide nanowires and nanorods synthesized by solvothermal method are very similar evidenced by the comparability of diffraction peaks in 2θ position and intensity. The two main diffraction peaks of both products can be well indexed to the monoclinic phase of $W_{18}O_{49}$ with lattice parameters of $a = 18.32$ Å, $b = 3.79$ Å, $c = 14.04$ Å and $\beta = 115.04°$ (JCPDS No. 65-1291). Also observe that there are no other impurity phase peaks. The strongest peak intensity of (0 1 0) plane indicates that the growth is preferentially along the b-axis, i.e. the [0 1 0] direction. In the present experiments, the monoclinic $W_{18}O_{49}$ structures obtained in the solvent of cyclohexanol and 1-propanol are identical (see the same diffraction peaks of monoclinic $W_{18}O_{49}$ in Fig. 3). It has been reported that one-dimensional nanostructures can be obtained by controlling the supersaturation of the precursors below a certain level in vapor-phase and solvothermal processes [23]. A low supersaturation is beneficial to the anisotropic growth of

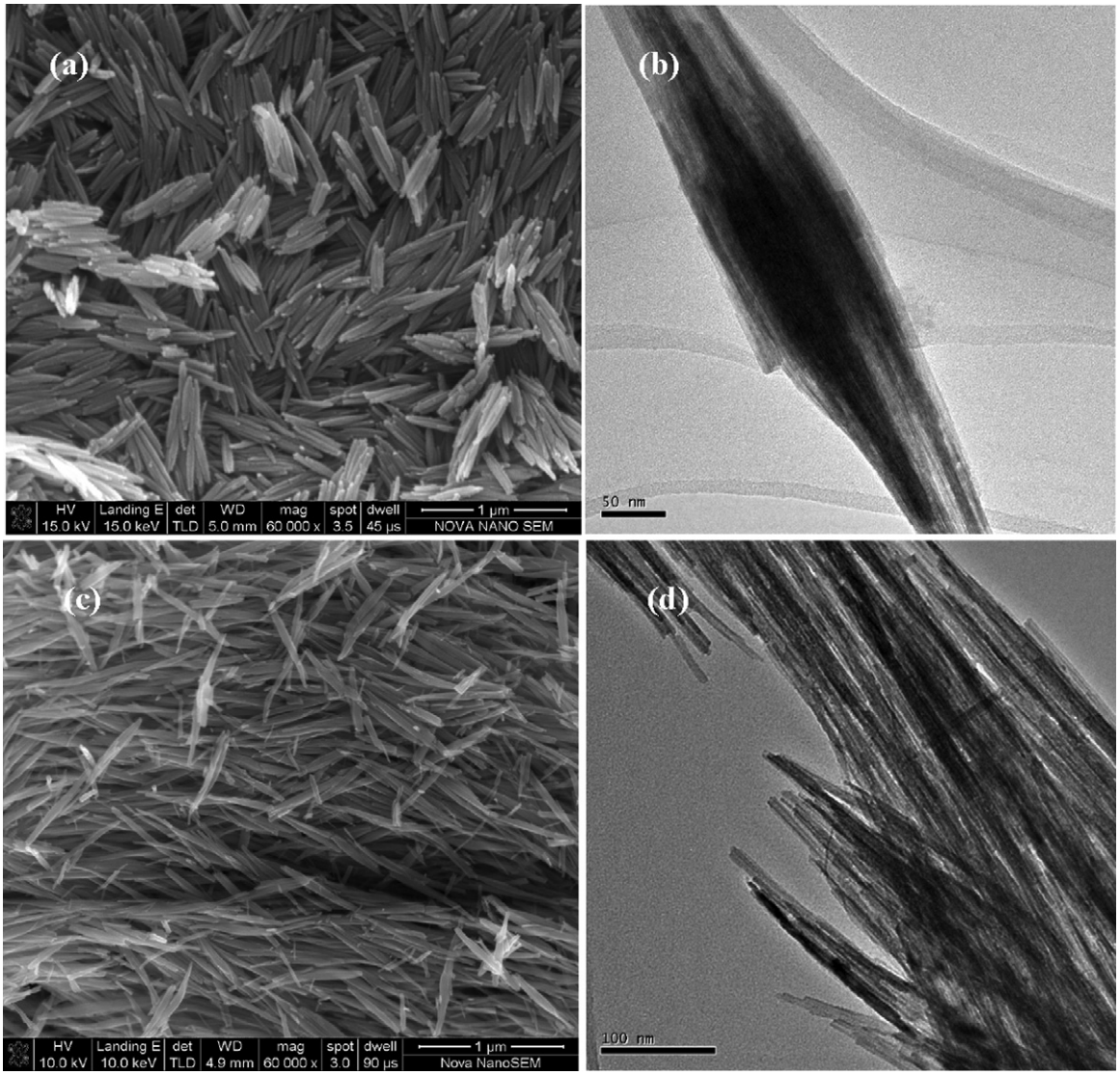

Fig. 2. (a) SEM and (b) TEM images of the nanorods synthesized in cyclohexanol at 200 °C for 6 h, (c) SEM and (d) TEM images of the nanowires synthesized in 1-propanol at 200 °C for 9 h.

the crystal whereas a medium or a high supersaturation supports bulk crystal or powder growth. In our work, the low solution concentration of 0.005 M might have contributed to the low supersaturation of the tungsten source, promoting the formation of the one-dimensional tungsten oxide. The high resolution (HR) TEM images of the nanorod and nanowire are shown in Fig. 4(a) and (b). Here, the lattice spacings for nanorod and nanowire are 0.378 nm and 0.380 nm, respectively, which correspond to (0 1 0) plane of monoclinic $W_{18}O_{49}$ according to JCPDS No. 65-1291. This result indicates that the annealed one-dimensional nanostructures all consist of monoclinic $W_{18}O_{49}$ and the dominant growth direction is along the *b*-axis direction, which is in agreement with the XRD results.

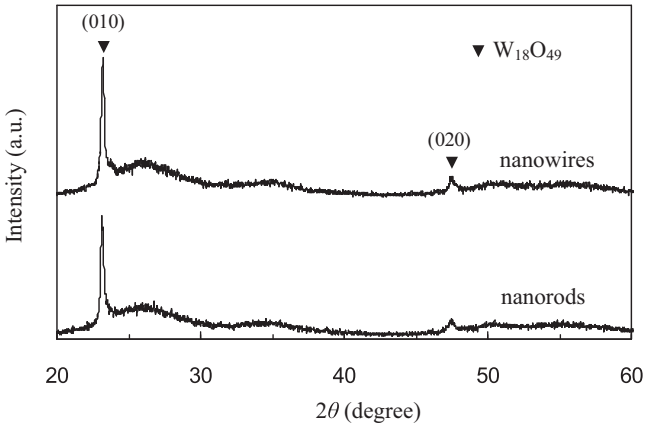

Fig. 3. XRD patterns of the products after annealing at 300 °C for 1 h.

XPS was carried out to investigate the chemical state of the $W_{18}O_{49}$ nanorods and nanowires. XPS spectra obtained are shown in Fig. 5, highlighted with the survey and the high-resolution spectra of W4f peaks. Tungsten is identified in the survey spectrum (see Fig. 5(a)) by the presence of the W4f, W4d, and W4p transitions. Also labeled are the O KLL and O1s features. The existing C1s line probably came from the surface contamination during the annealing treatment or the residue of organic solvent after annealing. Fig. 5(b) shows the high-resolution spectra of the W4f region, which contains the $W4f_{7/2}$ and $W4f_{5/2}$ peaks with binding energies of 35.2 eV and 37.2 eV respectively for nanorods and nanowires. In the previous report [24], the fully oxidized tungsten oxide (WO_3) has the doublet due to $W4f_{7/2}$ at 35.85 eV and $W4f_{5/2}$ at 38 eV,

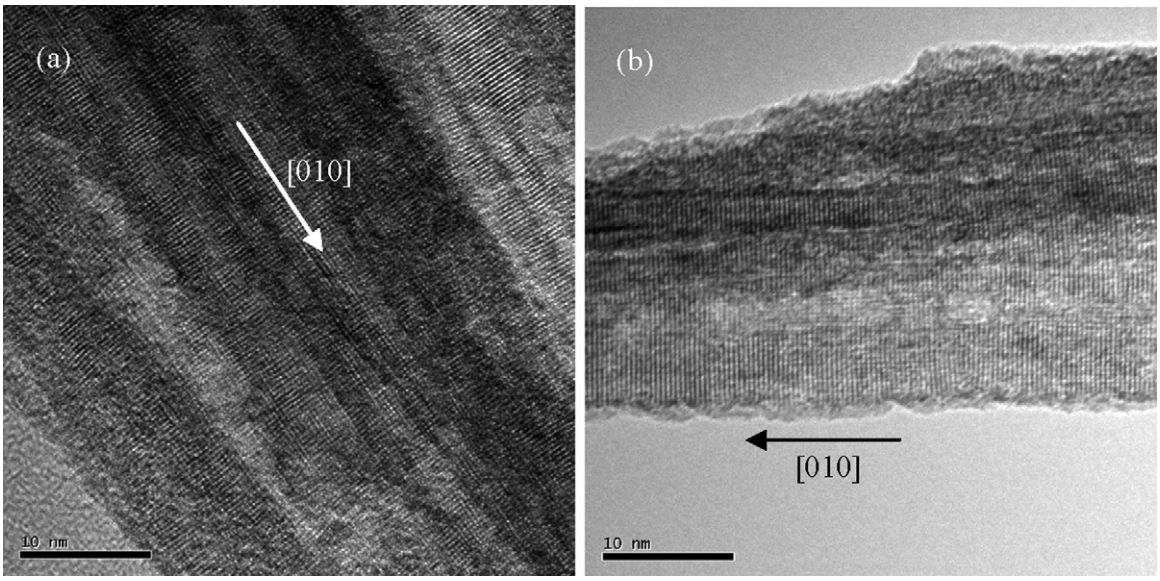

Fig. 4. HR-TEM images of (a) individual nanorod synthesized in cyclohexanol at 200 °C for 6 h, (b) individual nanowire synthesized in 1-propanol at 200 °C for 9 h.

which represents the W^{6+}. In Fig. 5(b), the position shift of the peaks corresponding to $W4f_{7/2}$ and $W4f_{5/2}$ indicates that the valence of tungsten in the nanorods and nanowires is unsaturated and there exist some oxygen vacancies. Because the electron density depends on the density of oxygen vacancies, the vacancies play a significant role in the detection mechanism for the oxide semiconductors [25]. Therefore, the existence of oxygen vacancies in the structure of tungsten oxide nanorods and nanowires is beneficial to the adsorption and reaction of gas molecules on their surface, consequently leading to much better gas sensing properties. From Fig. 5(b), it is also observed that, for the nanorods and nanowires, the binding energies for the peaks of $W4f_{7/2}$ and $W4f_{5/2}$ are the same, which suggests the same W valence. This result is consistent with the one of XRD measurements that nanorod and nanowire have the same crystalline structure of monoclinic $W_{18}O_{49}$.

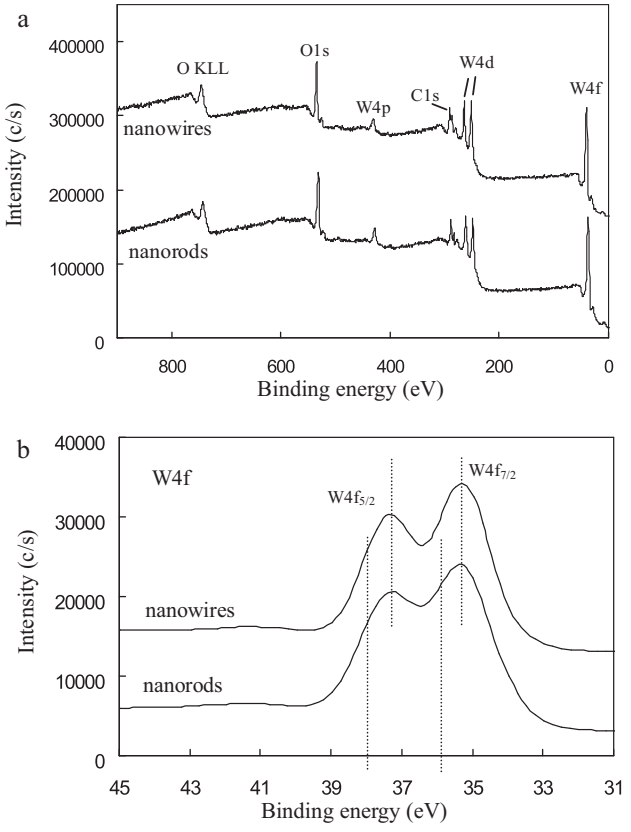

Fig. 5. The survey XPS spectra (a) and the W4f high-resolution XPS spectra (b) of tungsten oxide nanorods and nanowires.

3.2. Gas-response measurements

The NO_2-sensing properties of $W_{18}O_{49}$ nanorods and nanowires were tested. Fig. 6(a) and (b) shows the changes in the resistance of $W_{18}O_{49}$ nanorod and nanowire gas sensors upon exposure to NO_2 gas at an operating temperature of 200 °C. As shown in these fig-

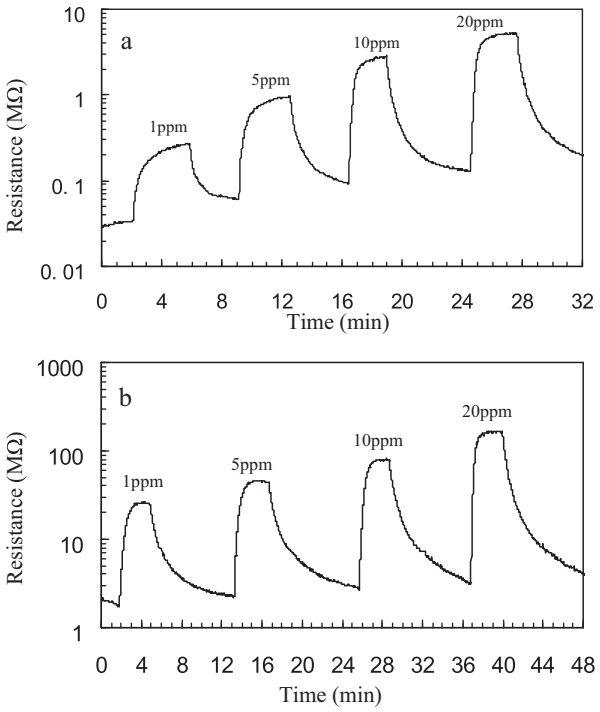

Fig. 6. Changes in the resistance of $W_{18}O_{49}$ nanorod (a) and nanowire (b) sensors upon exposure to 1, 5, 10 and 20 ppm NO_2 gas at an operating temperature of 200 °C.

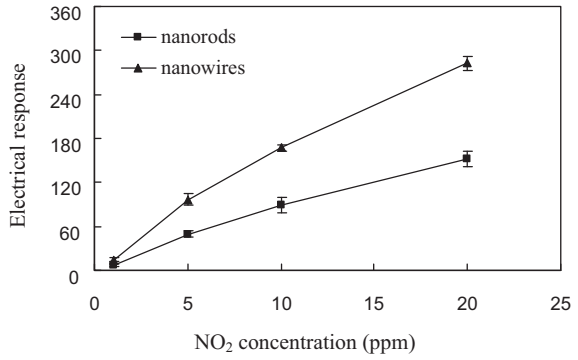

Fig. 7. Electrical responses of tungsten oxide nanorod and nanowire sensors as a function of NO_2 concentration at an operating temperature of 200 °C.

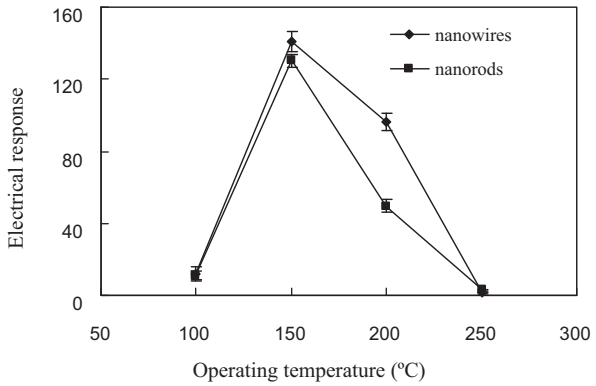

Fig. 9. Relationship between the sensor electrical responses and operating temperature for tungsten oxide nanowires and nanorods to 5 ppm NO_2.

ures, the measured resistance increased upon exposure to NO_2 gas. This result is expected because the oxidizing analyte NO_2 withdraws electrons from the n-type tungsten oxide surface, leading to the increase of sensor resistance [26]. It can be observed from Fig. 6(a) that there exists insufficient recovery of the resistance for the nanorods sensor after NO_2 gas releasing for 1000s. To fully recover the baseline value, more time would be needed. Differing from the nanorods sensor, the resistance of the nanowires sensor nearly recovers to its initial value after NO_2 removal, indicating a good reversibility of this type sensor.

The electrical responses of tungsten oxide nanowires and nanorods sensors to different concentrations of NO_2 at 200 °C are shown in Fig. 7. It should be noted that three different sensor samples were fabricated for each type of the sensors in order to ensure the reliability of the testing data. The gas-sensing properties of the three samples were found to be similar, indicating a good reproducibility. Every data shown in the following figures is the average value of three data obtained from the three sensor samples respectively. The error bars for each value were also shown in the figures. It can be seen from Fig. 7 that the responses of both sensors increase with the increasing of NO_2 gas concentration in the range of 1–20 ppm. Furthermore, the nanowires sensor exhibits higher gas response than the nanorods sensor when both are exposed to the same concentration of NO_2. Fig. 8 shows the response time curve of the sensors based on $W_{18}O_{49}$ nanowires and nanorods to 1–20 ppm NO_2 at 200 °C. Here, the response time is defined as the time required for the resistance to reach 90% of the equilibrium value after the test gas is injected. As shown in this figure, the response times vary in the range of 22–72 s for the nanowires, whereas for the nanorods the response times are 70–152 s. Thus, the nanorods show slower response compared

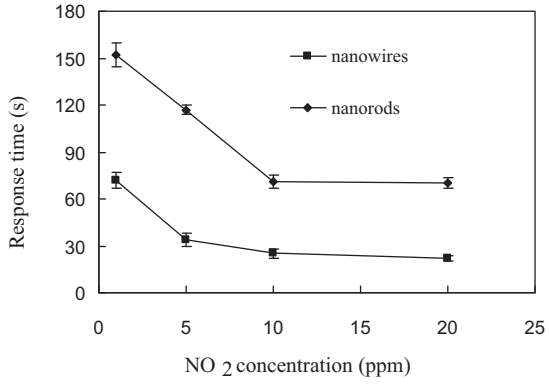

Fig. 8. Response time curve of $W_{18}O_{49}$ nanowires and nanorods sensors to different NO_2 concentration at an operating temperature of 200 °C.

to the nanowires. Nevertheless, considering the results reported for the tungsten oxide nanoparticles and sputtered films [17,27], the values of response time for the one-dimensional nanowires or nanorods are relatively satisfactory.

It is known that the gas-sensing mechanism of the oxide materials belongs to the surface-controlled type in which the grain size, surface states and oxygen adsorption play an important role [28,29]. For the n-type semiconductor oxide, the adsorbed oxygen molecules capture electrons from the conduction band of the sensing metal oxide and transform into oxygen ions (O^-, O^{2-} and $O_2{}^-$), creating a thin electron-depleted space-charge layer at the surface of the oxide. When the oxide is exposed to the target gas, the gas interacts either with the material or the preadsorbed oxygen at the surface. Since NO_2 is an oxidizing agent, changes in material resistance should be mainly caused by gas-tungsten oxide chemisorption processes rather than chemical bonds with atomic oxygen [30]. Therefore, NO_2 was adsorbed onto tungsten oxide surface and the oxygen of NO_2 acts as an acceptor, extracting electrons from the conduction band of the oxide, according to the following equations [31–33].

$$NO_2\,(gas) + e^- \rightarrow NO_2{}^-\,(ads) \quad (1)$$

$$NO_2\,(gas) + 0.5O_2\,(gas) + e^- \rightarrow NO_3{}^-\,(ads) \quad (2)$$

The formation of $NO_2{}^-$ (ads) and/or $NO_3{}^-$ (ads) besides negatively charged oxygen adsorbates (O^-, O^{2-} and $O_2{}^-$), leads to an increase of the electron-depleted layer, and then an increase in the potential barrier height at grain boundaries. In the case of n-type tungsten oxide nanorod or nanowire, it is thought that the proportion of the depleted volume in the total volume of the nanowire/nanorod increases rapidly with decreasing diameter and increasing specific surface area. Particularly, for thin tungsten oxide nanowire, a whole region can be occupied by the electron-depleted layer upon NO_2 adsorption, i.e., full depletion can occur, due to its large specific surface area and small lateral dimension. This can significantly increase the heights of the double Schottky barriers at the boundaries of the nanostructures, resulting in a large increase in the resistance and then a high electrical response. According to the BET measurements, the thin and long nanowires showed much larger specific surface area (83.65 m^2/g) than the short and thick nanorods (69.24 m^2/g). The larger surface area provides a larger amount of surface active sites for the oxygen and NO_2 adsorption. Thus, thinner nanowire shows much larger change in resistance upon exposure to NO_2 than the thicker nanorod.

To clarify the dependence of the sensor electrical response on the operation temperature, the resistances of $W_{18}O_{49}$ nanorod and nanowire sensors before and after the introduction of 5 ppm NO_2 at operating temperatures ranging from 100 °C to 250 °C were measured. Fig. 9 illustrates the relationship between the electri-

cal response and the operating temperature. In the range of the operating temperatures studied, from 100 to 250 °C, the electrical responses of the two sensors increased sharply at first and then decreased rapidly with increasing in the operating temperature. The responses show maximum values of 140.7 and 131.5 at 150 °C for the nanowires and nanorods, respectively. When operating temperature is above 150 °C, the nanowires and nanorods lose their responses quickly. Particularly, for $W_{18}O_{49}$ nanowires, the response value at 250 °C is only 1.26, which is less than one percent of that at 150 °C. The above results show that the operating temperature is one of the most important parameters affecting the sensor response. The electrical responses of the semiconductor oxide sensors come from the change in the resistance due to the chemisorbed oxygen and target analyte [28]. When exposed to NO_2 gas, the resistance of tungsten oxide can be changed due to the adsorption of NO_2 and atmospheric oxygen molecules on the surface. It is well known that adsorption and desorption are temperature-activated processes, and the surface coverage is also temperature dependent [34]. At low temperature, the amount of chemisorbed oxygen and NO_2 species on the inactive surface of oxide is small. Conversely, some of the adsorbed species may be desorbed from the surface at high temperature. From Fig. 9, the measurements carried out at temperatures ranging from 150 °C to 200 °C obtain relative perfect electrical responses. The highest response value is achieved at 150 °C.

Selectivity is an important factor for the practical application of gas sensor. In order to study the selectivity of the tungsten oxide nanowires and nanorods sensors, the gas responses of the sensors to 5 ppm NO_2, 200 ppm NH_3 and 200 ppm ethanol were tested at 200 °C. The results indicated that the gas response values to 5 ppm NO_2 of nanowires and nanorods sensors at 200 °C were 96.3 and 49.7 respectively, which were markedly higher than those to NH_3 (1.11 and 1.17 respectively) and ethanol (1.88 and 1.75 respectively). Here, the sensor response to reducing NH_3 and ethanol was calculated by R_0/R_g value. Therefore, highly selective detection of NO_2 gas can be realized by the one-dimensional tungsten oxide sensors.

4. Conclusions

$W_{18}O_{49}$ nanorods and nanowires were synthesized at 200 °C by solvothermal method. Both the nanorods and nanowires exhibit bundle features, as observed by SEM and TEM analyses. BET method was used to evaluate the specific surface area of the tungsten oxide. The long and thin nanowires show higher specific surface area (83.65 m^2/g) than the short and thick nanorods (69.24 m^2/g). The NO_2-sensing properties of $W_{18}O_{49}$ nanorods and nanowires were tested using a static gas sensing characterization system. Both sensors exhibited good selectivity to NO_2 gas at 200 °C. In comparison with nanorods, the nanowires showed a much shorter response time and a relative higher response value to NO_2 gas. Nevertheless, the response time for the one-dimensional nanowires or nanorods are much shorter than the tungsten oxide nanoparticles and sputtered films reported in the literatures. The results indicate that the one-dimensional tungsten oxide nanostructures, particularly $W_{18}O_{49}$ nanowires structure is a promising gas-sensing material for high performance NO_2 gas sensor.

Acknowledgments

This work was financially supported by the National Natural Science Foundation (No. 60801018), Tianjin Natural Science Foundation (No. 09JCYBJC01100) and the New Teacher Foundation of Ministry of Education of China (No. 200800561109).

References

[1] G. Eranna, B.C. Joshi, D.P. Runthala, R.P. Gupta, Crit. Rev. Solid State Mater. Sci. 29 (2004) 111–188.
[2] G.N. Chaudhari, A.M. Bende, A.B. Bodade, S.S. Patil, V.S. Sapkal, Sens. Actuators B 115 (2006) 297–302.
[3] B. Timmer, W. Olthuis, A. Berg, Sens. Actuators B 107 (2005) 666–677.
[4] G. Korotcenkov, I. Blinov, M. Ivanov, J.R. Stetter, Sens. Actuators B 120 (2007) 679–686.
[5] Y.K. Chung, M.H. Kim, W.S. Um, H.S. Lee, J.K.S. Song, Ch. Choi, K.M. Yi, M.J. Lee, K.W. Chung, Sens. Actuators B 60 (1999) 49–55.
[6] Y.B. Shen, T. Yamazaki, Z.F. Liu, D. Meng, T. Kikuta, N. Nakatani, Thin Solid Films 517 (2009) 2069–2072.
[7] Z.W. Pan, Z.R. Dai, Z.L. Wang, Science 291 (2001) 1947–1949.
[8] Y. Cui, C.M. Lieber, Science 291 (2001) 851–853.
[9] A. Kolmakov, D.O. Klenov, Y. Lilach, S. Stemmer, M. Moskovits, Nano Lett. 5 (2005) 667–673.
[10] A.S. Zuruzi, A. Kolmakov, N.C. Macdonald, M. Moskovits, Appl. Phys. Lett. 88 (2006) 102904.
[11] A.Z. Sadek, W. Wlodarski, Y.X. Li, W. Yu, X. Li, X. Yu, K. Kalantar-zadeh, Thin Solid Films 515 (2007) 8705–8708.
[12] C.Y. Wang, M. Ali, T. Kups, C.-C. Röhlig, V. Climalla, T. Stauden, O. Ambacher, Sens. Actuators B 130 (2008) 589–593.
[13] Z.F. Liu, T. Yamazaki, Y.B. Shen, T. Kikuta, N. Nakatani, Y.X. Li, Sens. Actuators B 129 (2008) 666–670.
[14] L.C. Tien, P.W. Sadik, D.P. Norton, L.F. Voss, S.J. Pearton, H.T. Wang, B.S. Kang, F. Ren, J. Jun, J. Lin, Appl. Phys. Lett. 87 (2005) 222106.
[15] J. Pollleux, A. Gurlo, N. Barsan, U. Weimar, M. Antonietti, M. Niederberger, Angew. Chem. Int. Ed. 45 (2006) 261–265.
[16] Y.G. Choi, G. Sakai, K. Shimanoe, N. Yamazoe, Sens. Actuators B 101 (2004) 107–111.
[17] Z.F. Liu, T. Yamazaki, Y.B. Shen, T. Kikuta, N. Nakatani, Sens. Actuators B 128 (2007) 173–178.
[18] J. Jimenez, J. Arbiol, G. Dezanneau, A. Cornet, J.R. Morante, Sens. Actuators B 93 (2003) 475–485.
[19] B. Zhang, J.D. Liu, S.K. Guan, Y.Z. Wang, Y.Z. Zhang, R.F. Chen, J. Alloys Compd. 439 (2007) 55–58.
[20] C.S. Rout, M. Hegde, C.N.R. Rao, Sens. Actuators B 128 (2008) 488–493.
[21] R.A. Gerlitz, K.D. Benkstein, D.L. Lahr, J.L. Hertz, C.B. Montgomery, J.E. Bonevich, S. Semancik, M.J. Tarlov, Sens. Actuators B 136 (2009) 257–264.
[22] R.F. Mo, G.Q. Jin, X.Y. Guo, Mater. Lett. 61 (2007) 3787–3790.
[23] Y.N. Xia, P.D. Yang, Y.G. Sun, Y.Y. Wu, B. Mayers, B. Gates, Y.D. Yin, F. Kim, H.Q. Yan, Adv. Mater. 15 (2003) 353–389.
[24] C.G. Grandqvist, Handbook of Inorganic Electrochromics Materials, Elsevier, Amsterdam, 1995.
[25] W. Gopel, K.D. Schierbaum, Sens. Actuators B 26–27 (1995) 1–12.
[26] C.O. Park, S.A. Akbar, J. Mater. Sci. 38 (2003) 4611–4637.
[27] T. Kida, A. Nishiyama, M. Yuasa, K. Shimanoe, N. Yamazoe, Sens. Actuators B 135 (2009) 568–574.
[28] M.E. Franke, T.J. Koplin, U. Simon, Small 2 (2006) 36–50.
[29] A. Rothschild, Y. Komem, J. Appl. Phys. 95 (2004) 6374–6380.
[30] E. Rossinyol, A. Prim, E. Pellicer, J. Rodríguez, F. Peiró, A. Cornet, J.R. Morante, B. Tian, T. Bo, D. Zhao, Sens. Actuators B 126 (2007) 18–23.
[31] Z. Hua, Y. Wang, H. Wang, L. Dong, Sens. Actuators B 150 (2010) 588–593.
[32] C. Zhang, M. Debliquy, A. Boudiba, H. Liao, C. Coddet, Sens. Actuators B 144 (2010) 280–288.
[33] S.H. Wang, T.C. Chou, C.C. Liu, Sens. Actuators B 94 (2003) 343–351.
[34] J. Mizsei, Sens. Actuators B 23 (1995) 173–176.